International Journal of Safety and Security Engineering
Vol. 16, No. 4, April, 2026, pp. 899-912
Journal homepage: http://iieta.org/journals/ijsse

Conjugate Heat Transfer Benchmarking of Refinery Tank Insulation in Coastal Outdoor Exposure

Hatem T M Duhair[1], Jamil Abedalrahim Jamil Alsayaydeh[1], Mazen Farid[2,3*], Abdulmumin Amhimmid Salim Abu Sayf[4], Safarudin Gazali Herawan[5]

[1] Department of Engineering Technology, Fakulti Teknologi Dan Kejuruteraan Elektronik Dan Komputer (FTKEK), Universiti Teknikal Malaysia Melaka, Melaka 75450, Malaysia
[2] Faculty of Information Science and Technology (FIST), Multimedia University, Melaka 75450, Malaysia
[3] Centre for Intelligent Cloud Computing, COE for Advanced Cloud, Multimedia University, Melaka 75450, Malaysia
[4] Fakulti Teknologi Maklumat dan Komunikasi, Universiti Teknikal Malaysia Melaka, Melaka 75450, Malaysia
[5] Industrial Engineering Department, Faculty of Engineering, Bina Nusantara University, Jakarta 11480, Indonesia

Corresponding Author Email: ramadhan.mazen@mmu.edu.my

https://doi.org/10.18280/ijsse.160417

Received: 29 January 2026
Revised: 8 March 2026
Accepted: 13 March 2026
Available online: 30 April 2026

Keywords:
refinery storage tanks, thermal insulation, conjugate heat transfer, ANSYS fluent, coastal exposure, heat loss reduction, techno-economic screening, corrosion under insulation

ABSTRACT

Outdoor refinery tanks act as large heat exchangers, and the resulting heat loss has consequences that extend beyond energy use to outer-surface temperature control and insulation-system integrity. This study presents a controlled conjugate heat transfer benchmark of three insulation families for a heated storage tank in ANSYS Fluent: aerogel composite blanket, polyurethane foam, and cellular glass. The computational domain includes the steel wall and insulation only, while the outdoor environment is represented through a mixed convection-radiation boundary with prescribed ambient forcing, constant material properties, and ideal bonded interfaces. Single-layer designs are evaluated at 50, 100, and 150 mm, together with a 150 mm three-layer stack composed of one 50 mm layer of each insulation family. At 24 h, the uninsulated reference heat flux is 783.77 W/m². With insulation, the flux falls to 13.401, 25.145, and 47.915 W/m² at 50 mm, and to 5.315, 10.769, and 21.044 W/m² at 150 mm, for aerogel, polyurethane, and cellular glass, respectively. The ranking remains unchanged across thickness, and the gain beyond 100 mm becomes progressively smaller, indicating a practical thickness knee under the stated forcing assumptions. A preliminary screening index based on indicative cost per heat flux saved identifies polyurethane foam as the most attractive compromise within this setup, while aerogel remains the thermal best with a cost premium and cellular glass remains relevant where moisture tolerance and long-term stability are prioritised.

1. INTRODUCTION

Tank farms are essential to refinery continuity because production, blending, and shipment rarely proceed at the same pace. Yet the same tanks also create a persistent thermal and integrity burden. A heated storage tank behaves as a large exposed heat-transfer surface, and every avoidable watt lost through the shell must be replaced by fuel, steam, or electricity. That replacement duty is not only a cost. It also sustains elevated shell temperatures, increases the consequence of insulation damage, and can leave local hot surfaces that matter during inspection rounds and routine operator access.

For above-ground tanks, the heat path is conceptually simple and operationally difficult. Heat conducts through the steel wall and insulation, then leaves the outer surface through convection and radiation. Those external terms do not remain fixed. Wind, solar loading, and night-sky exchange change through the day, and even modest differences in boundary representation can alter predicted storage heat load and the apparent benefit of insulation [1, 2]. In exposed coastal service, this variation is not a rare disturbance. It is part of the normal operating envelope.

This is why refinery insulation cannot be judged by nominal conductivity alone. Porous insulation performance shifts with moisture, temperature, density, airflow, and aging, so the conductivity used in design may not be the conductivity sustained in service. Reviews of insulation behaviour consistently identify moisture and temperature as dominant drivers of thermal drift, with additional variation introduced by environmental exposure over time [3, 4]. In practice, the signal is often indirect. A system may appear visually intact while the plant records higher heat duty, less stable product temperature, or both.

Moisture ingress makes the problem more serious because it couples heat loss to corrosion risk. A failed seam, damaged cladding lap, or degraded sealant can admit rain, humid air, or condensate into the insulation system. Once moisture is retained, the steel surface may remain wet for extended periods, which supports corrosion under insulation and reduces the thermal resistance that the insulation was supposed

to provide. Experimental work on water transport and drying in insulated systems shows that once water bypasses the weather barrier, wetness persistence is governed by coupled evaporation and adsorption processes rather than by simple drainage alone [5, 6]. A damaged cladding seam left untreated through one wet season is a concrete example: the same defect can increase heat leakage, prolong time of wetness, and hide corrosion activity beneath an apparently minor exterior flaw.

Material choice therefore has direct engineering and safety implications. Aerogel composite blankets are attractive where high resistance per unit thickness is needed, and reported conductivity ranges place them among the strongest thermal performers in this class [7]. Polyurethane foam remains appealing because it is lightweight and widely deployable, but its effective conductivity can change with temperature, humidity, and aging associated with gas diffusion in closed cells [8]. Cellular glass occupies a different position. It is commonly selected where moisture tolerance is central, because its closed-cell structure limits water ingress even though its conductivity is typically higher than that of aerogel and new polyurethane systems [9]. These materials are not interchangeable in refinery service, and the preferred option depends on which operational constraint dominates, minimum heat loss, thickness limitation, moisture tolerance, long-term stability, or some combination of these [10, 11].

The Al-Zawiya refinery context helps explain why this comparison matters, but it should be read carefully. Outdoor tanks there operate within a coastal-arid exposure envelope in which ambient temperature can range from roughly 0 °C to 48 °C and relative humidity can approach 85% [12, 13]. Under such conditions, daily boundary forcing can materially affect heat loss, while any breach at joints or penetrations can initiate the moisture pathway that underlies corrosion under insulation [14, 15]. Corrosion under insulation is widely recognised as external corrosion that develops when water penetrates the insulation system and reaches the steel surface [16], and its management remains difficult because deterioration progresses with limited visual evidence until inspection or failure reveals it [17, 18]. Safety concerns extend further because degraded insulation can also produce local hot surfaces that increase contact-burn risk during routine plant work [19]. For that reason, this study uses the Al-Zawiya setting as an operationally relevant exposure context, not as a fully parameterised plant-specific case study with resolved site flow physics [20].

The literature already provides several important foundations, but not the exact comparison needed here. Resistance-network methods and standards-based calculations remain the normal route for thickness selection because they are transparent and fast. General material reviews explain how conductivity varies with moisture, temperature, and aging. Corrosion-under-insulation studies clarify why moisture retention and time of wetness matter for integrity. What is less common is a controlled Computational Fluid Dynamics (CFD)-based, like-for-like comparison that isolates candidate insulation families under the same imposed forcing and reports decision-facing outputs, specifically late-time heat flux and outer-surface temperature, for an externally insulated refinery tank. That is the gap addressed in this paper.

Accordingly, this study develops a controlled numerical benchmark for three refinery-relevant insulation families, aerogel composite blanket, polyurethane foam, and cellular glass, applied to an externally insulated heated storage tank. The model resolves conduction through the steel wall and insulation, while the outdoor environment is imposed through a mixed convection-radiation boundary rather than through an explicitly solved external flow field. Thickness effects are examined at 50, 100, and 150 mm, and a 150 mm three-layer configuration is included to test whether layering offers a thermal advantage under ideal bonded contact. The main outputs are heat flux and outer-surface temperature, and these are then interpreted through a preliminary techno-economic screening layer suitable for early retrofit comparison rather than full plant-wide investment appraisal.

The contribution of the paper is therefore specific. It provides a controlled CFD comparison of three insulation families under identical forcing, quantifies thickness-related diminishing returns across a practical 50 to 150 mm range, tests a refinery-relevant multilayer concept against single-layer alternatives, and translates the thermal outputs into screening indicators that are meaningful for maintenance and integrity planning under the stated assumptions.

The sections that follow are organised accordingly: Section 2 reviews the relevant literature, Section 3 defines the model and boundary conditions, Section 4 presents the thermal and screening results, and Section 5 concludes with the practical implications and limitations of the benchmark.

2. RELATED WORKS

2.1 External boundary heat exchange in exposed tanks

Heat loss from outdoor tanks is controlled by a coupled boundary problem rather than by conduction alone. Even when product temperature is maintained near a setpoint, the shell, roof, and base are exposed to different external conditions across the day, so conduction through steel and insulation interacts continuously with convection and radiation at the outer surface [21, 22]. For this reason, industrial design commonly begins with resistance-network methods, where steel and insulation are treated as series resistances and the internal and external surfaces are represented through heat-transfer coefficients and radiation terms. ISO 12241 formalises this framework for industrial installations and remains valuable because it offers a consistent basis for screening insulation thickness across many assets [23]. Yet the reliability of that screening still depends on how outdoor boundary terms are defined.

External convection is particularly sensitive to exposure. Wind, geometry, and buoyancy alter the atmospheric boundary layer around cylindrical equipment, which in turn changes the effective outer heat-transfer coefficient. Under low wind, free convection correlations are often used, while increasing wind shifts the problem toward forced convection, with practical formulations available for cylinders and related surfaces [24, 25]. Radiation adds an equally important pathway. Sky temperature does not coincide exactly with ambient air temperature, and radiative exchange can change materially with humidity and cloud cover even when the air temperature appears similar [2, 26]. Local discontinuities further complicate the picture. Supports, nozzles, joints, and geometric interruptions can bypass part of the nominal insulation resistance and produce thermal bridges that raise local heat flux and outer-surface temperature [27, 28]. In operational terms, this matters because a localised warm region can signal either a geometrical heat-loss pathway or the early presence of insulation deterioration.

This body of work supports the use of a mixed convection-radiation boundary in the present model, because the aim is not to treat the outer coefficient as a fixed material constant, but to represent the exposed tank wall as a boundary-value problem under controlled forcing.

2.2 In-service material behaviour and property drift

The second theme concerns what insulation materials actually do in service. Reported dry conductivity values are useful starting points, but they do not fully represent field performance once moisture, temperature variation, aging, and installation constraints begin to act together [29, 30]. Experimental and review studies show that moisture content can increase effective thermal conductivity markedly, while the joint effect of temperature and moisture can further shift the apparent thermal resistance seen by the system [31, 32]. Measurement itself becomes more difficult when moisture redistributes under a thermal gradient, because equilibrium conditions are hard to maintain and heat-flow estimates become sensitive to transient internal redistribution [33]. This is one reason why an insulation system that appears acceptable on a datasheet may perform differently after months of outdoor exposure.

Among the materials relevant to refinery service, aerogel composite blankets, polyurethane foams, and cellular glass represent three distinct strategies. Aerogel blankets are attractive where high thermal resistance must be achieved within limited thickness, and the literature consistently supports their value in retrofit applications around congested details and appurtenances [34, 35]. Their behaviour is still exposure-dependent. Hydrophobic composites reduce liquid uptake, but effective conductivity can drift when composite structure, moisture history, or installation quality changes [36, 37]. Polyurethane foam offers strong initial thermal performance and flexible manufacturing routes, yet long-term behaviour depends on aging, gas diffusion, and the success of water exclusion at interfaces and joints [38-40]. Cellular glass occupies a different position. Its closed-cell structure and very low water absorption make it attractive where moisture tolerance and property stability dominate the decision, even though its dry conductivity is usually higher than that of aerogel and new polyurethane systems [41, 42].

This literature justifies the decision to compare three insulation families with clearly different conductivity, moisture sensitivity, and lifecycle behaviour, rather than treating insulation choice as a single-variable thickness problem.

2.3 Wet insulation, corrosion under insulation, and operational risk

A third body of literature links thermal performance to integrity. In refinery environments, wet insulation is not simply a thermal defect. It is a precursor condition for corrosion under insulation, because retained water can keep the steel surface wet for long enough to support hidden degradation. Modelling and experimental studies show that moisture migration through porous insulation can alter apparent conductivity and heat flow under wetting and drying cycles, especially when the material retains water or dries slowly [43]. This matters in exposed coastal service, where repeated dew-point crossings, humid air, and rain ingress can extend time of wetness once the cladding system is breached.

Mitigation is therefore framed in layered terms. One line of defence seeks to exclude water through proper jacketing, sealing, and detailing. A second seeks to limit retention if water enters, by using hydrophobic or non-absorbent materials where possible [44]. A third focuses on detection. Thermography, radiography, and guided-wave approaches are increasingly discussed as practical screening tools for wet insulation or metal loss without extensive removal [45]. Coatings beneath insulation remain important because perfect exclusion is unrealistic at refinery scale, and drying can be delayed substantially when venting is limited or the insulation microstructure traps moisture [2, 46]. A simple operational example illustrates the mechanism: a minor opening at a cladding seam can admit water during one wet season, create a thermally anomalous strip on the exterior, and at the same time maintain a concealed wet zone against the steel surface.

This literature supports the paper's emphasis on heat flux and outer-surface temperature as operationally meaningful outputs, because both variables relate not only to energy loss but also to the early reading of wet zones, elevated surface hazard, and corrosion-related exposure.

2.4 Industrial selection and thickness optimization

The final theme concerns how engineers move from thermal physics to practical specification. Standard-based resistance methods remain the main route for industrial thickness selection because they are transparent, fast, and reproducible, and ISO-based approaches are still widely used for screening across multiple assets [47]. At the same time, optimum-thickness studies show that thickness selection is rarely governed by heat loss alone. The thermal benefit of added thickness eventually weakens as external resistances begin to limit further reduction, while material and installation costs continue to rise. This produces the familiar diminishing-return behaviour seen in insulation economics and explains why the lowest heat flux is not always the most rational design choice when budget, geometry, maintenance access, and service durability are considered together.

That trade-off becomes sharper when the material families differ not only in conductivity but also in ageing pathway, water tolerance, and installation form. Aerogel can justify a thinner retrofit where clearance is limited. Polyurethane can become attractive where a lower first cost is needed with strong thermal benefit. Cellular glass can remain defensible when moisture tolerance and long-term stability are treated as constraints rather than secondary preferences [34-42]. This selection logic is closer to refinery practice than a simple ranking by conductivity, because engineers often accept a somewhat higher steady heat loss if the selected system reduces inspection burden, simplifies detailing, or lowers the likelihood of persistent wet insulation zones.

This literature supports two choices in the present study: first, the inclusion of multiple thickness levels to reveal the practical knee in performance, and second, the addition of a preliminary screening layer that interprets the thermal results in a form closer to early retrofit decision-making.

Taken together, these four strands of literature define the need for the present work. Standard methods remain essential for traceable thickness selection, but they compress a spatially and temporally variable boundary problem into simplified coefficients. Material studies explain why dry conductivity alone cannot represent field behaviour. Corrosion-under-insulation research shows that moisture retention changes the

meaning of thermal degradation from an efficiency issue into an integrity issue. Selection studies indicate that thickness and material choice must be read as a trade-space rather than a single ranking exercise. On that basis, the present paper adopts a controlled conjugate heat transfer benchmark in which candidate insulation families are compared under identical mixed convection-radiation forcing using decision-relevant outputs, namely heat flux and outer-surface temperature. Table 1 summarises the comparative property envelope of the three insulation families considered in this work, with emphasis on conductivity, moisture sensitivity, mechanical form, and lifecycle concerns.

Table 1. Comparative property envelope of candidate insulation families

Attribute (Typical)	Aerogel Composite Blanket	PU/PIR Rigid Foam	Cellular Glass (Foam Glass Family)
Thermal conductivity, dry, near 20 °C	0.013–0.020 [36, 41]	0.020–0.030 when new, increases with aging [37]	0.038–0.050 [48, 49]
Moisture sensitivity (in service)	Reduced liquid uptake in hydrophobic composites, k can still shift with exposure [36]	Performance depends strongly on water exclusion and aging pathways [37]	Low water uptake supports stable properties under wet exposure [49, 50]
Typical mechanical form	Flexible blanket, retrofit-friendly [36]	Spray, panel, or shell systems [37]	Rigid blocks or segments [49]
Key lifecycle concern	Maintain hydrophobic integrity and jacketing quality	Aging and interface moisture pathways	Joint sealing, brittleness, installation labor

Note: PU = polyurethane; PIR = polyisocyanurate

3. METHODOLOGY

3.1 Case definition and insulation matrix

This study evaluates heat loss from an externally insulated heated storage tank using a controlled three-dimensional conjugate heat transfer model developed in ANSYS Fluent. The purpose of the model is comparative rather than plant-wide predictive. It resolves heat conduction through the steel shell and insulation system, while the outdoor environment is imposed through a mixed convection-radiation boundary at the exposed outer surface. This formulation allows the effect of insulation material and thickness to be compared under identical forcing, which is the main requirement of the present benchmark.

The tank geometry was reconstructed from the project design basis and represented as a vertical cylindrical tank with a diameter of 6.16 m and a height of 7.38 m. The shell was modelled as carbon steel with a wall thickness of 8 mm. Three insulation families were considered as single-layer systems: aerogel composite blanket, polyurethane foam, and cellular glass. Each material was evaluated at three total thicknesses, 50, 100, and 150 mm. In addition, one multilayer configuration was assessed at a total thickness of 150 mm using three 50 mm layers arranged from the tank wall to the ambient side as follows: aerogel composite blanket, polyurethane foam, and cellular glass. Stating the order explicitly is essential because the temperature gradient and effective resistance distribution depend on the layer sequence when the materials differ substantially in conductivity. The overall model geometry and the applied thermal boundaries are shown in Figure 1, while the implemented wall and insulation build-up is presented in Figure 2. The material properties used in the baseline CFD model are listed in Table 2, and the full insulation configuration matrix is summarised in Table 3.

The insulation matrix was selected to address two practical design questions. The first concerns the relative performance of the three materials when applied individually at the same thickness. The second concerns whether a mixed-layer assembly provides a thermal advantage over the best single-layer alternative under ideal bonded contact. The 50 mm configuration was retained because moderate thicknesses are often the first realistic option in retrofit settings where nozzles, cladding details, or access constraints limit the available build-up.

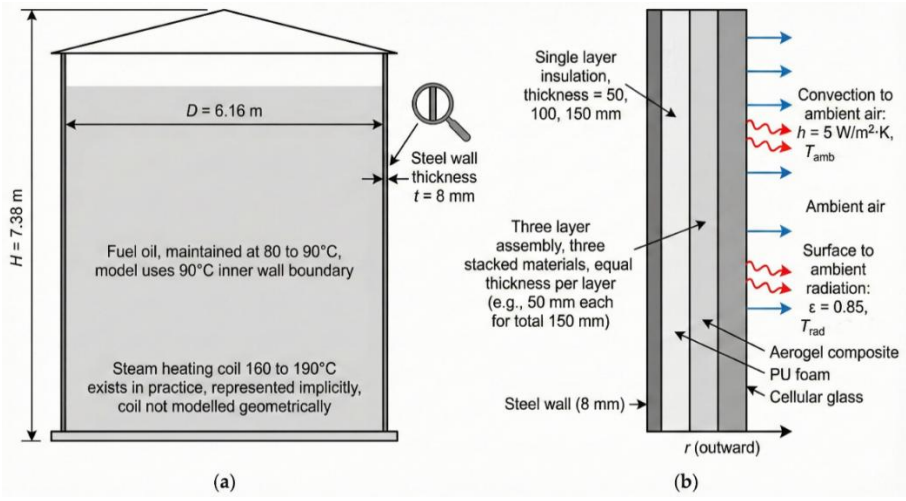

Figure 1. Geometry and boundary conditions used in ANSYS Fluent Al-Zawiya refinery heated fuel-oil tank

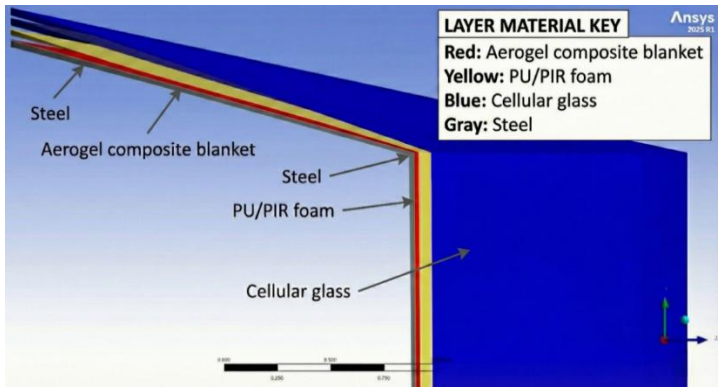

Figure 2. ANSYS model geometry showing the tank wall and insulation layers configuration

Table 2. Material properties used in the Computational Fluid Dynamics (CFD) baseline (constant properties)

Material	Density (kg m^{-3})	Conductivity (w m^{-1} k^{-1})	Specific Heat (j kg^{-1} k^{-1})
Aerogel composite	120	0.013	1273
Polyurethane foam	30	0.025	1400
Cellular glass	136	0.05	800
Carbon steel (a283)	7850	51	470
Concrete	2300	1.4	880

Table 3. Insulation configurations examined

Configuration	Total Thickness	Layer Definition (From Tank Wall to Ambient)	Thickness per Layer	Purpose
Aerogel only	50, 100, 150 mm	Aerogel composite blanket	50, 100, 150 mm	Single-material benchmark
PU only	50, 100, 150 mm	Polyurethane foam	50, 100, 150 mm	Single-material benchmark
Cellular glass only	50, 100, 150 mm	Cellular glass	50, 100, 150 mm	Single-material benchmark
Hybrid 3-layer stack	150 mm	Aerogel / Polyurethane / Cellular glass	50 mm + 50 mm + 50 mm	Multilayer comparative case

Note: PU = polyurethane

3.2 Material assumptions and interface treatment

The material properties used in the CFD model were held constant within each simulation. This assumption was adopted to establish a controlled thermal baseline and to isolate the influence of insulation selection from other factors such as moisture uptake, aging, gas diffusion in polymer foams, or interface degradation. The resulting rankings should therefore be interpreted as rankings under dry conditions with ideal layer contact rather than as full field-service predictions.

Heat transfer is formulated as transient conduction in solids with continuity of temperature and heat flux at material interfaces. In ANSYS Fluent, this is implemented through coupled wall interfaces at the steel-insulation boundary. Interfaces between adjacent layers in the hybrid configuration are treated as perfectly bonded and free of explicit contact resistance. This assumption prevents installation-dependent contact conductance from obscuring the material-family comparison, and it defines the multilayer case as an ideal thermal baseline rather than a worst-case installation scenario. The adopted conductivity magnitudes and the relative ranking of aerogel composite blanket, polyurethane foam, and cellular glass are consistent with reported ranges for these material classes [51-53].

3.3 Governing formulation and boundary conditions

Heat transfer within the tank wall and insulation system was modelled as transient conduction in solid domains. The internal hot-side condition was imposed directly at the inner steel wall, while the external boundary was represented through combined convection and radiation. The outward surface heat flux can be written as

$$q'' = h_{conv}(T_s - T_\infty) + \varepsilon\sigma(T_s^4 - T_{rad}^4) \quad (1)$$

where, q'' is the outward heat flux per unit area, h_{conv} is the external convective heat-transfer coefficient, T_s is the outer surface temperature, T_∞ is the ambient air temperature, ε is the surface emissivity, σ is the Stefan-Boltzmann constant, and T_{rad} is the effective radiative surrounding temperature.

Table 4. Boundary-condition set used in the Computational Fluid Dynamics (CFD) baseline

Quantity	Symbol	Value	Unit	Applied Location	Modelling Note
Inner wall temperature	T_{in}	90	°C	Inner steel wall	Constant hot-side boundary
Ambient temperature	T_∞	25	°C	Outer insulation surface	Baseline and transient reference
External convection coefficient	h_{conv}	5	W m^{-2} K^{-1}	Outer insulation surface	Constant across all cases
Surface emissivity	ε	0.85	-	Outer insulation surface	Constant across all cases
Radiation temperature	T_{rad}	25	°C	Outer insulation surface	Assumed equal to ambient
Simulation duration	t	86,400	s	Whole domain	24 h transient run

Table 5. Forcing schedule used in the transient simulations

Time Range	Ambient Temperature
0 to 24 h	25 °C

The internal wall temperature was fixed at 90 °C to represent hot-service operation. At the external insulation surface, convection was represented by a constant heat-transfer coefficient of 5 W m^{-2} K^{-1}, and surface emissivity was set to 0.85. The radiative surrounding temperature was taken equal to the ambient reference temperature. The baseline ambient temperature was 25 °C. For clarity and reproducibility, the complete boundary-condition set is reported in Table 4, and the forcing schedule used in the documented transient simulations is stated explicitly in Table 5. The representative external film coefficient was selected in a manner consistent with standard cylinder heat-transfer correlations used to translate outdoor exposure into an effective boundary condition when the airflow domain is not solved explicitly [54].

The transient simulation window was set to 24 h, corresponding to 86,400 s. As documented in the uploaded files, the ambient condition remained at 25 °C over the full 24 h period. This point is stated directly here so that the paper no longer implies an hourly forcing profile that is not numerically reported. All insulation cases were therefore compared under the same constant thermal forcing over the 24 h transient window, allowing late-time heat flux and surface temperature to be reported on a consistent basis.

3.4 Numerical setup, mesh strategy, and convergence control

All simulations were executed in ANSYS Fluent using a three-dimensional heat-transfer formulation in which only the energy equation is solved within the solid regions, and the environment is imposed through the mixed convection–radiation boundary. Spatial discretisation uses second-order schemes for the energy equation. Time integration uses an implicit transient scheme.

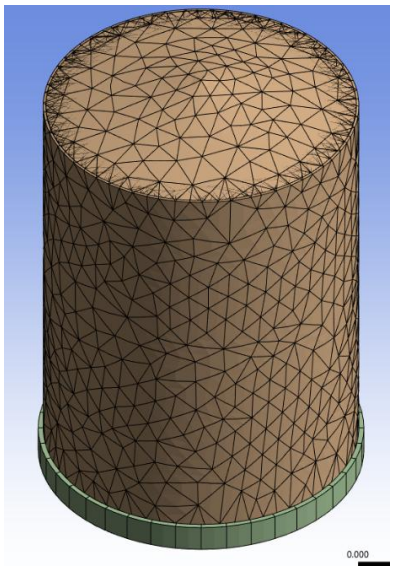

Figure 3. Mesh refinement using ANSYS for the insulator

Transient simulations were marched to 86,400 s (24 h) to resolve the conductive response under diurnal forcing and to confirm stabilisation of the reported heat-flux and surface-temperature metrics. Time-step selection was chosen to be materially smaller than the forcing interval (1 h). A sensitivity check was performed to confirm that reducing the time step further does not change the monitored outputs beyond the mesh-study tolerance.

The mesh was designed to resolve the dominant through-thickness gradients in the steel wall and insulation layers. Refinement was concentrated near the inner wall, the steel-insulation interface, the interfaces between insulation layers in the hybrid case, and the exposed outer surface where heat exchange with the environment occurs. A conformal mesh was maintained across all bonded interfaces [55, 56]. This arrangement is appropriate for layered conduction problems because it minimises numerical smearing and captures the thermal drop across each material with greater fidelity. The local refinement pattern adopted for the insulation model is shown in Figure 3.

Convergence at each time step is assessed using a dual criterion: residual reduction for the energy equation and stability of engineering monitors. The monitors include area-averaged outer heat flux, maximum and average outer surface temperature, and layer-by-layer temperature drops. This matters because the decision variables are integrated quantities, and residuals alone can be misleading in conduction-dominated simulations [57].

3.5 Verification and reproducibility controls

To strengthen reproducibility, three checks were used: analytical consistency, mesh independence, and time-step independence. The analytical check compared the CFD prediction with a cylindrical thermal-resistance calculation under the same boundary assumptions. The deviation was evaluated using

$$\text{Deviation}(\%) = \frac{| q''_{\text{CFD}} - q''_{\text{analytical}} |}{q''_{\text{analytical}}} \times 100 \qquad (2)$$

A mesh-refinement study was then performed using coarse, medium, and fine grids. Acceptance was based on monotonic convergence and a change of less than 2% in the main reported outputs between successive refinement levels. A similar criterion was applied in the time-step study, where three time increments smaller than the reporting interval were compared. The grid-refinement and verification workflow adopted in the study is summarised in Figure 4, while the resulting numerical checks are consolidated in Table 6. This verification structure follows common practice in discretisation-uncertainty and grid-convergence reporting for CFD-based thermal studies.

The verification results indicate close agreement between the analytical resistance model and the CFD solution, with a heat-flux deviation of 1.02%, which remains within the adopted acceptance band. The mesh study shows stable monotonic convergence, while the time-step study confirms that the reported 24 h thermal outputs are insensitive to further temporal refinement within the selected range. On this basis, the medium mesh and the 600 s production time step were retained for the full simulation matrix because they provided stable predictions at lower computational cost than the finest settings.

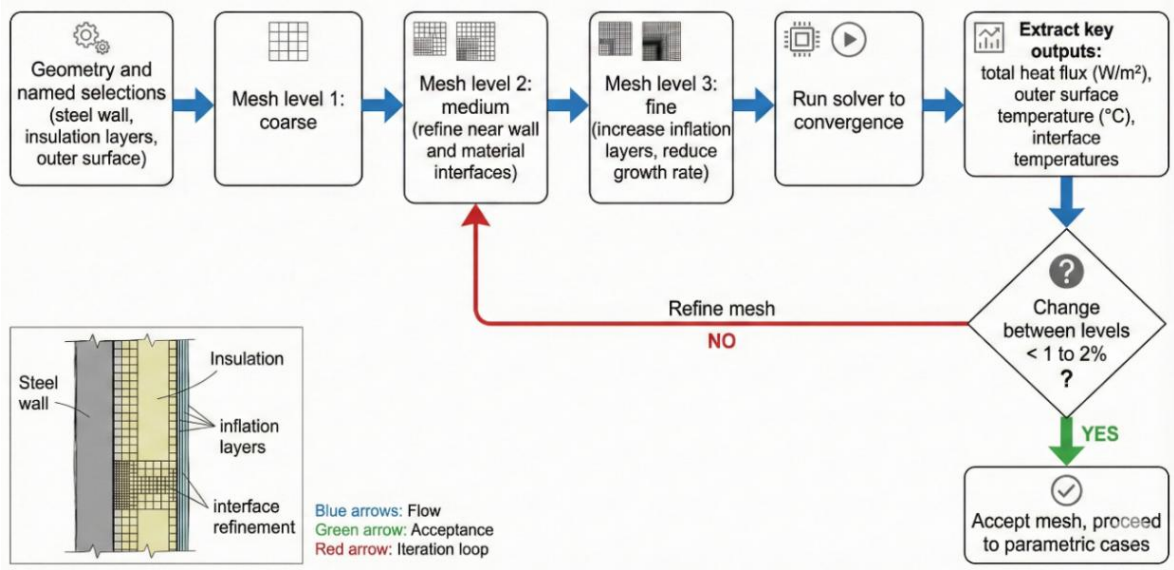

Figure 4. Mesh refinement and grid independence workflow for the tank insulation model

Table 6. Verification summary for analytical consistency, mesh independence, and time-step independence

Check	Case Used	Setting	Heat Flux at 24 h (W m^{-2})	Outer Surface Temperature at 24 h (°C)	Change from Previous Level (%)	Acceptance Criterion	Outcome
Analytical consistency	Polyurethane foam, 50 mm	Analytical model	25.41	30.98	-	Deviation < 2%	Pass
Analytical consistency	Polyurethane foam, 50 mm	Computational Fluid Dynamics (CFD)	25.15	30.95	1.02	Deviation < 2%	Pass
Mesh study	Polyurethane foam, 50 mm	Coarse mesh	24.83	30.84	-	$\Delta q'' < 2\%$, $\Delta Ts < 2\%$	Pass
Mesh study	Polyurethane foam, 50 mm	Medium mesh	25.05	30.91	0.89	$\Delta q'' < 2\%$, $\Delta Ts < 2\%$	Pass
Mesh study	Polyurethane foam, 50 mm	Fine mesh	25.15	30.95	0.40	$\Delta q'' < 2\%$, $\Delta Ts < 2\%$	Pass
Time-step study	Polyurethane foam, 50 mm	Δt = 900 s	25.22	30.97	-	$\Delta q'' < 2\%$, $\Delta Ts < 2\%$	Pass
Time-step study	Polyurethane foam, 50 mm	Δt = 600 s	25.18	30.96	0.16	$\Delta q'' < 2\%$, $\Delta Ts < 2\%$	Pass
Time-step study	Polyurethane foam, 50 mm	Δt = 300 s	25.15	30.95	0.12	$\Delta q'' < 2\%$, $\Delta Ts < 2\%$	Pass

3.6 Output extraction and economic framing

All cases were post-processed using the same reporting convention. The inner reference corresponds to the imposed hot-side wall temperature. For the uninsulated case, the outer wall corresponds directly to the exposed steel surface. For insulated cases, temperatures were also extracted at the steel-insulation interface and, in the hybrid case, at each internal layer boundary. This layer-by-layer reporting is important because it shows how the thermal gradient is redistributed when multiple materials are combined.

Three primary outputs were extracted from the simulations: local and area-averaged outer heat flux, local and area-averaged outer-surface temperature, and total heat loss obtained by integrating heat flux over the external tank surface. These quantities were selected because they connect directly to the engineering questions of the study. Heat flux represents the continuing thermal penalty of hot storage. Outer-surface temperature relates to surface safety and the practical thermal behaviour of the insulation system. The comparison at 24 h was used as the main reporting point because it reflects the late-time condition under identical forcing for all cases.

The economic interpretation of the results was kept at screening level. Present-worth notation was used to maintain a consistent economic basis:

$$PV = \frac{C_t}{(1+r)^t} \tag{3}$$

$$LCC = C_0 + \sum_{t=1}^{n} \frac{C_t}{(1+r)^t} \tag{4}$$

where, PV is present value, C_t is the cost or saving at time t, r is the discount rate, C_0 is the initial investment, and $n$is the evaluation horizon [58]. In the present study, however, the economic comparison is intentionally limited to a preliminary screening perspective derived from the CFD thermal outputs. It is not presented as a full refinery-wide techno-economic appraisal, which would require site-specific installation cost, labor, maintenance frequency, degradation history, and downtime exposure.

4. RESULTS AND DISCUSSION

4.1 Baseline reference and reporting convention

Before comparing insulation options, the output definitions used throughout the results must be fixed clearly. The reporting surfaces and extracted thermal outputs are illustrated in Figure 5, which defines the inner reference, the outer reporting surface, and the direction of the extracted heat flux. The uninsulated reference case is then presented in Figure 6, which provides the baseline checkpoints for heat flux and external wall temperature against which all reductions are calculated.

The baseline case confirms the severity of uninsulated operation. At 24 h, the external heat flux remains 783.77 W/m², which means the steel wall behaves as an efficient heat-loss surface under the imposed mixed convection-radiation boundary. This baseline is important because all percentage reductions and all screening metrics reported later are referenced to this condition. It also provides the physical context for the insulation results. The question is not whether insulation helps, because even thin insulation does that decisively. The real comparison is how much additional benefit is obtained as the material family and thickness change under the same forcing.

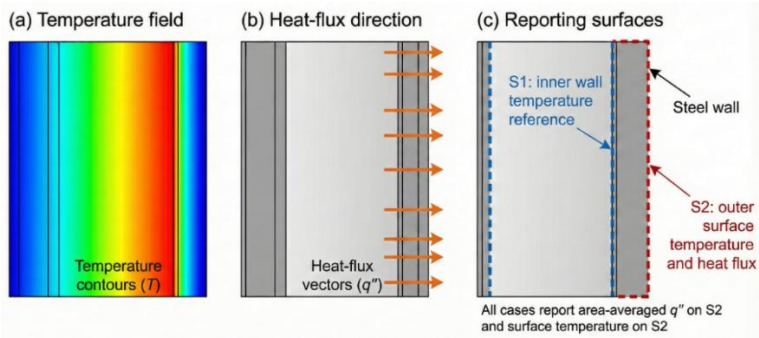

Figure 5. Post-processing outputs and reporting definitions used for comparing insulation cases

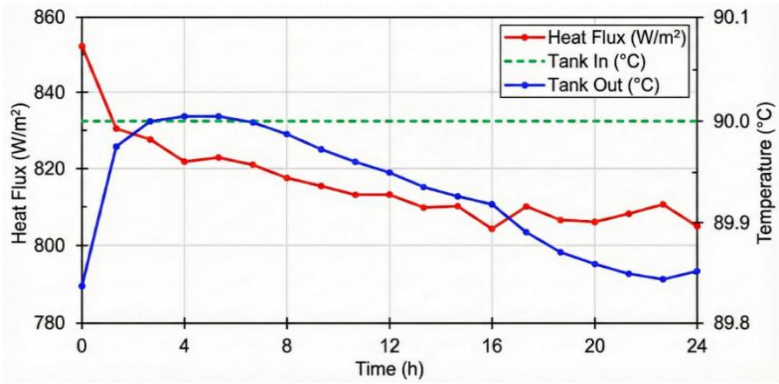

Figure 6. Baseline (no insulation) reference checkpoints for heat flux and external wall temperature

4.2 Single-layer insulation performance, thickness effect, and ranking stability

The late-time heat-flux comparison for the single-layer cases is shown in Figure 7, while the corresponding temperature drop across the wall and insulation layers is shown in Figure 8. Together, these two figures establish the main thermal findings of the study.

Adding a single insulation layer reduces the late-time heat flux by roughly one to two orders of magnitude relative to the uninsulated reference, depending on material and thickness. More importantly, the ranking by heat flux is stable at every thickness. Aerogel composite blanket gives the lowest heat flux, polyurethane foam remains intermediate, and cellular glass is consistently highest. At 50 mm, the 24 h heat flux is 13.401 W/m² for aerogel, 25.145 W/m² for polyurethane foam, and 47.915 W/m² for cellular glass. At 100 mm, the values fall to 9.672, 18.307, and 35.352 W/m², respectively. At 150 mm, they fall further to 5.315, 10.769, and 21.044 W/m². Expressed relative to the uninsulated baseline, the reductions are already very large at 50 mm, namely 98.29% for aerogel, 96.79% for polyurethane foam, and 93.89% for cellular glass. At 150 mm, the reductions reach 99.32%, 98.63%, and 97.32%, respectively.

The central engineering point is not simply that thicker insulation performs better. It is that the incremental improvement weakens beyond 100 mm, even though the total heat flux still decreases. This is the practical thickness knee that matters in refinery retrofit work, where nozzle clearance, cladding complexity, inspection access, and installation cost often constrain the design envelope [59]. The step from 50 to 100 mm yields a clear improvement in both heat flux and surface temperature. The step from 100 to 150 mm remains thermally beneficial, but the marginal gain is smaller because the external boundary, especially convection and radiation at the exposed surface, begins to limit how much additional thickness can reduce the final heat loss.

The temperature results support the same interpretation. The inner reported surface remains close to 90 °C in all single-layer cases, which confirms that differences arise from the insulation system rather than variation in the hot-side condition. The outer surface temperature decreases as

thickness increases, shifting more of the temperature drop into the insulation where it belongs. At 50 mm, the outer surface lies approximately at 42.4 ℃ for aerogel, 43.5 ℃ for polyurethane foam, and 45.6 ℃ for cellular glass. At 100 mm, the three materials converge near the mid-30 ℃ band, around 35.6 ℃. At 150 mm, aerogel remains near 35.1 ℃, polyurethane foam near 35.8 ℃, and cellular glass near 38.2 ℃. This convergence in surface temperature, even while heat-flux ranking remains stable, is physically reasonable. Once the outer surface approaches the ambient-dominated exchange regime, additional internal resistance still lowers heat flux, but the exposed surface temperature cannot fall indefinitely because the external convection-radiation boundary sets a lower limit.

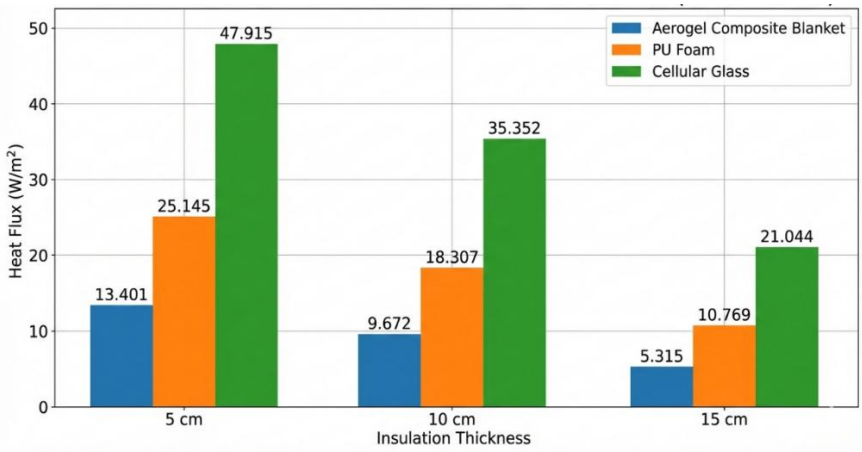

Figure 7. Reported steady heat flux rate versus total insulation thickness for single-layer materials

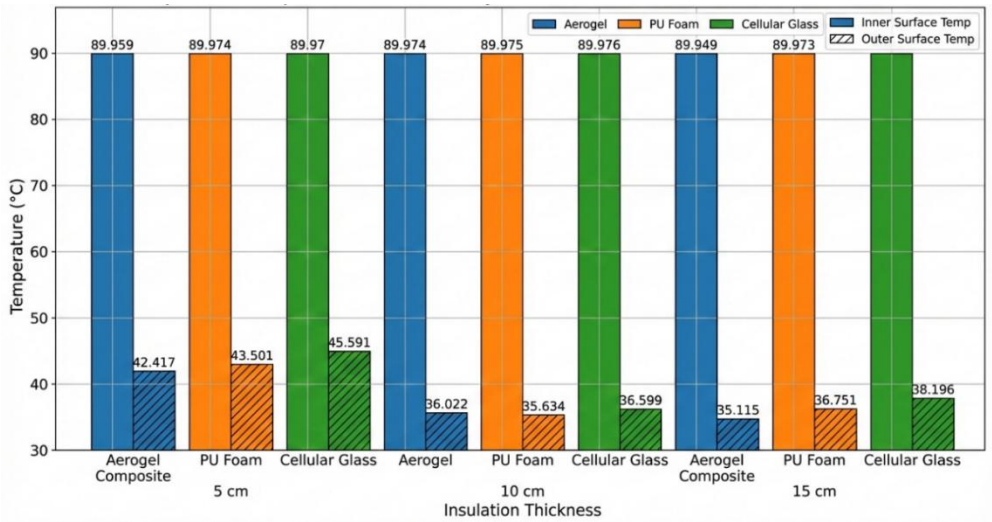

Figure 8. Temperature drop across insulation layers at different thicknesses (24 simulation)

4.3 Multilayer assemblies and transient response

The multilayer case was introduced to test whether stacking dissimilar materials could provide a useful thermal advantage at a total thickness of 150 mm. The transient evolution of the hybrid assembly is presented in Figure 9, and the outer-surface temperature field at 24 h is shown in Figure 10.

The transient curves show a physically consistent response. “Tank In” remains close to 90 ℃, which confirms that the hot-side boundary is tightly controlled. “Tank Out” remains only slightly lower, while the temperatures at the insulation interfaces separate gradually and approach quasi-steady values over the 24 h window. This means that the temperature gradients are being contained within the insulation stack rather than propagating strongly to the external surface. By the end of the simulation, the outermost hybrid surface remains close to the ambient range, which is operationally relevant for touch safety and external surface control.

The most important result, however, is the final heat flux. At 24 h, the hybrid 150 mm stack gives 25.307 W/m². This value is almost identical to the 50 mm polyurethane foam case, which gives 25.145 W/m², and it is substantially higher than the 150 mm single-layer cases, especially aerogel at 5.315 W/m² and polyurethane foam at 10.769 W/m². This is the non-intuitive result that requires a direct explanation.

The explanation is straightforward once the stack is interpreted as a series thermal-resistance problem. Under quasi-steady conduction, the same heat flux passes through all layers, while the total resistance is the sum of the layer resistances, $R = \sum L/k$. In the present hybrid stack, one-third of the total thickness is assigned to cellular glass, which has the highest conductivity among the three materials used. That higher-conductivity layer contributes less resistance per unit thickness than aerogel or polyurethane foam. As a result, the total resistance of the 150 mm hybrid assembly is pulled downward toward the moderate range rather than remaining close to the best single-material 150 mm designs. In other words, the stack does not create a thermal synergy simply by

combining three materials. It averages their resistances. Even under ideal bonded contact, replacing part of a 150 mm low-conductivity insulation system with a higher-conductivity layer reduces the total thermal resistance and therefore raises the final heat flux.

This point matters operationally. The hybrid configuration may still be justified for reasons of constructability, moisture tolerance, surface-temperature targets, or exposure management. But under the stated assumptions of constant properties and ideal interfaces, it should not be described as thermally superior to a full-thickness low-conductivity single-layer system. Its value is practical and system-oriented, not a purely thermal optimisation.

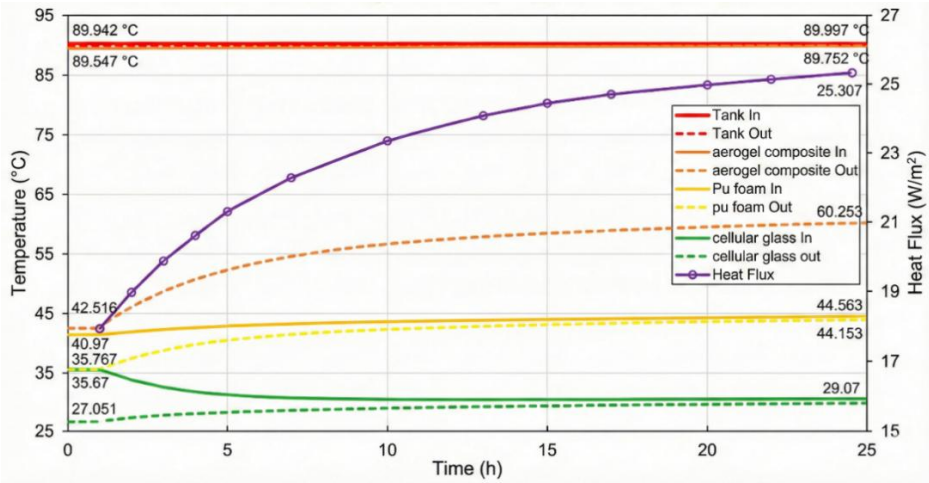

Figure 9. 24 h transient response for the three layer configuration, showing bulk tank temperature (Tank In, Tank Out), layer interface temperatures ("In" and "Out" faces for each layer), and total external heat flux

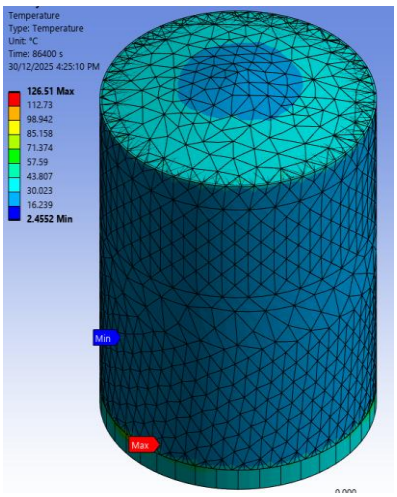

Figure 10. Temperature field on the tank external surface at 24 h for the 3 layer, 50 mm per layer insulation configuration

4.4 Screening interpretation and consolidated performance summary feasibility, design implication, and selection summary

Thermal ranking alone does not determine a refinery retrofit decision. Insulation is purchased, installed, inspected, repaired, and eventually replaced, so the decision should be read through both thermal performance and comparative cost. For that reason, the results are summarised in one screening table that combines the main decision-facing metrics, namely heat flux at 24 h, outer-surface temperature, percentage reduction relative to the baseline, and indicative cost per saved heat flux. This screening logic is transparent and reproducible, but it remains a screening layer, not a full plant-specific investment model [60, 61].

Three selection patterns follow directly from Table 7. First, the aerogel composite blanket is the technical best performer at every thickness. It gives the lowest heat flux and the largest percentage reduction, but this comes with a strong cost premium, especially once thickness increases beyond 100 mm and the incremental thermal gain becomes small. Second, polyurethane foam provides the strongest performance-to-cost compromise in this screening. Even at 50 mm it achieves a 96.79% reduction, and its cost per saved heat flux remains the lowest across the material set. Third, cellular glass occupies the durability end of the design trade-space. Its heat flux is consistently higher than that of aerogel and polyurethane foam at equal thickness, but it still delivers large absolute reductions and remains defensible where moisture tolerance, dimensional stability, and long-term service behaviour are treated as governing constraints rather than secondary preferences.

Thickness should therefore be interpreted through marginal gain, not only through absolute reduction. The 50 mm cases already remove most of the baseline heat loss. The step to 100 mm gives a clear additional reduction in both heat flux and outer-surface temperature. The step from 100 to 150 mm still improves performance, but the marginal benefit is weaker and should be justified through site-specific objectives such as touch-temperature control, available clearance, long-term exposure conditions, or maintenance strategy [60, 61].

4.5 Interpretation under the stated assumptions

These results are most useful when read as a controlled thermal baseline rather than as a complete field-performance validation. The model uses constant material properties, ideal bonded interfaces, a prescribed internal wall temperature, and a fixed mixed convection-radiation boundary. Under those stated assumptions, the ranking by heat flux is clear, the thickness knee beyond 100 mm is visible, and the hybrid result shows that layering unlike materials does not guarantee a thermal advantage.

That scope does not reduce the engineering value of the study. It clarifies it. Under the stated assumptions, the results

provide a reproducible basis for comparing insulation families in terms of heat-loss control, outer-surface temperature, and preliminary retrofit screening. What they do not establish on their own is full field robustness under variable wind, changing emissivity, moisture ingress, aging, or imperfect contact. For that reason, statements about coastal exposure, safety relevance, and economic preference should be read as selection guidance within the defined model envelope, not as proof of universal superiority under all refinery conditions.

Table 7. Consolidated thermal and screening summary at 24 h

Configuration	Thickness (mm)	Heat Flux at 24 h (W/m²)	Outer-Surface Temperature (°C)	Heat-Flux Reduction (%)	Indicative Cost (RM/m²)	Cost per Saved Heat Flux, RM per (W/m²)
No insulation	0	783.770	Baseline reference	0.00	0	-
Aerogel composite blanket	50	13.401	42.4	98.29	450	0.584
Aerogel composite blanket	100	9.672	35.6	98.77	900	1.163
Aerogel composite blanket	150	5.315	35.1	99.32	1350	1.734
Polyurethane foam	50	25.145	43.5	96.79	35	0.046
Polyurethane foam	100	18.307	35.6	97.66	70	0.091
Polyurethane foam	150	10.769	35.8	98.63	105	0.136
Cellular glass	50	47.915	45.6	93.89	70	0.095
Cellular glass	100	35.352	35.6	95.49	140	0.187
Cellular glass	150	21.044	38.2	97.32	210	0.275
Hybrid, aerogel / polyurethane / cellular glass	150	25.307	Near ambient range	96.77	555	0.732

5. CONCLUSION

This work developed a controlled CFD benchmark for comparing three refinery-relevant insulation families, aerogel composite blanket, polyurethane foam, and cellular glass, for an externally insulated heated storage tank under a consistent mixed convection-radiation boundary. The uninsulated reference confirmed the severity of baseline heat loss, with a 24 h external heat flux of 783.77 W/m². Once insulation was introduced, heat flux dropped sharply and the ranking by thermal performance remained stable across thickness. Aerogel composite blanket gave the lowest heat flux at every thickness, polyurethane foam remained intermediate, and cellular glass was consistently higher.

A second practical finding was the presence of a clear thickness knee. Increasing thickness from 50 to 100 mm produced a strong additional reduction in heat flux and outer-surface temperature. Increasing thickness from 100 to 150 mm remained beneficial, but the marginal gain weakened because the external convection-radiation boundary increasingly limited further improvement. Under the stated assumptions, this makes the 100 mm range a credible engineering compromise for many retrofit settings, especially where thermal benefit, constructability, and material use must be balanced together.

The multilayer 150 mm configuration provided an important cautionary result. Although it combined three insulation families, its final heat flux, 25.307 W/m², was essentially equal to the 50 mm polyurethane foam case and clearly above the 150 mm single-layer aerogel and polyurethane cases. Under the stated assumptions, the hybrid assembly did not produce a purely thermal advantage, because the inclusion of a higher-conductivity layer reduced the total thermal resistance of the stack. Its justification, therefore, lies in system-level considerations such as constructability, moisture tolerance, or exposure management, not in an assumed thermal synergy.

When interpreted through a preliminary screening metric, polyurethane foam emerged as the most attractive performance-to-cost compromise, aerogel composite blanket remained the thermal best with a large cost premium, and cellular glass remained a defensible choice where durability and moisture resistance dominate the selection envelope. These conclusions should be read as a reproducible thermal baseline for comparison and early retrofit screening, not as a full plant-specific field validation. Future work should extend this baseline by introducing sensitivity to external coefficient variation, radiative conditions, interface resistance, and moisture-degraded conductivity so that ranking stability can be tested under more realistic service variability.

ACKNOWLEDGMENT

The authors express their gratitude to the Centre for Research and Innovation Management (CRIM) at Universiti Teknikal Malaysia Melaka (UTeM) for their valuable support in this research.

AUTHOR CONTRIBUTIONS

Conceptualization, J.A.J.A. and A.A.S.A.S.; methodology, H.T.M.D.; software, J.A.J.A.; validation, H.T.M.D.; formal analysis, M.F.; investigation, J.A.J.A.; resources, M.F.; data curation, J.A.J.A.; writing—original draft preparation, J.A.J.A. and S.G.H.; writing—review and editing, All authors; visualization, A.A.S.A.S.; supervision, M.F.; project administration, H.T.M.D.; funding acquisition, M.F. and S.G.H. All authors have read and agreed to the published version of the manuscript.

DATA AVAILABILITY

All the datasets used in this study are available from the Zenodo database (accession number: https://zenodo.org/records/19203371).

REFERENCES

[1] Liu, H., Wang, D., Liu, Y., Yin, T., Chen, Y. (2023). Heat loss characteristics and economic insulation optimization of solar storage tank in the extreme plateau climate. In Proceedings of the 5th International Conference on Building Energy and Environment. COBEE 2022, Environmental Science and Engineering. Springer, Singapore. https://doi.org/10.1007/978-981-19-9822-5_57

[2] Sun, W., Li, M.Y., Liu, Y.D., Cheng, Q.L., Zhao, L.X., Shao, S., Wang, Z.H. (2023). Study of main factors influencing unsteady-state temperature drop in oil tank storage under dynamic thermal environment coupling. Petroleum Science, 20(6): 3783-3797. https://doi.org/10.1016/j.petsci.2023.08.003

[3] Tariku, F., Molleti, S. (2023). Thermal performance of flat roof insulation materials: A review of temperature, moisture and aging effects. Journal of Building Engineering, 76: 107142. https://doi.org/10.1016/j.jobe.2023.107142

[4] Kendzierawska, W., Trochonowicz, M. (2024). Effect of temperature and humidity on the thermal conductivity λ of insulation materials. Civil and Environmental Engineering Reports, 33(4): 42-49. https://doi.org/10.59440/ceer/178976

[5] Dragovic, H., Damaceno, D.S., Meyer, O., Ervik, Å. (2024). Water transport and corrosion under insulation: Experimental investigations of drying in mineral wool. Process Safety and Environmental Protection, 190: 198-210. https://doi.org/10.1016/j.psep.2024.08.016

[6] Cao, Q., Pojtanabuntoeng, T., Esmaily, M., Thomas, S., Brameld, M., Amer, A., Birbilis, N. (2022). A review of corrosion under insulation: A critical issue in the oil and gas industry. Metals, 12(4): 561. https://doi.org/10.3390/met12040561

[7] Bommidi, A., Poorna Mohan, P., Naveen, P.N.E. (2019). Experimental analysis of thermal conductive properties on aerogel-filled composite structure. In Advances in Fluid and Thermal Engineering. Lecture Notes in Mechanical Engineering. Springer, Singapore. https://doi.org/10.1007/978-981-13-6416-7_64

[8] Andersons, J., Modniks, J., Kirpluks, M. (2021). Estimation of the effective diffusivity of blowing agents in closed-cell low-density polyurethane foams based on thermal aging data. Journal of Building Engineering, 44: 103365. https://doi.org/10.1016/J.JOBE.2021.103365

[9] El-Amir, A.A.M., Attia, M., Fend, T., Ewais, E.M.M. (2022). Synthesis of impermeable cellular glass foam from soda lime glass waste using SiC foaming agent. International Journal of Materials Technology and Innovation, 2(1): 1-4. https://doi.org/10.21608/ijmti.2022.97130.1038

[10] Anh, L.D.H., Anh, L.D.H., Anh, L.D.H., Pásztory, Z. (2021). An overview of factors influencing thermal conductivity of building insulation materials. Journal of Building Engineering, 44: 102604. https://doi.org/10.1016/J.JOBE.2021.102604

[11] Porzuczek, J. (2024). Comparative study on selected insulating materials for industrial piping. Materials, 17(7): 1601. https://doi.org/10.3390/ma17071601

[12] Sun, W., Cheng, Q., Sun, Z., Jiawei, F. (2018). Numerical simulation of heat flux in unsteady heat transfer for large floating-roof tanks. Chemistry and Technology of Fuels and Oils, 54(2): 219-230. https://doi.org/10.1007/S10553-018-0917-8

[13] Alsayaydeh, J.A.J., Indra, W.A., Khang, A.W.Y., Hossain, A.K.M.Z., Shkarupylo, V. and Pusppanathan, J. (2020). The experimental studies of the automatic control methods of magnetic separators performance by magnetic product. ARPN Journal of Engineering and Applied Sciences, 15(7): pp. 922-927

[14] Rahim, N.F.B.A., Khang, A.W.Y., Hassan, A., Elias, S.J., Gani, J.A.M., Jasmis, J. and Alsayaydeh, J.A.J. (2021). Channel congestion control in VANET for safety and non-safety communication: A review. In 2021 6th IEEE International Conference on Recent Advances and Innovations in Engineering (ICRAIE), Kedah, Malaysia, pp. 1-6. https://doi.org/10.1109/ICRAIE52900.2021.9704017

[15] Ifezue, D., Tobins, F.H., Nettikaden, V.C. (2014). CUI failure of a hot oil line due to intermittent operations. Journal of Failure Analysis and Prevention, 14(1): 13-16. https://doi.org/10.1007/S11668-013-9765-3

[16] Eltai, E.O., Musharavati, F., Mahdi, E. (2019). Severity of corrosion under insulation (CUI) to structures and strategies to detect it. Corrosion Reviews, 37(6): 553-564. https://doi.org/10.1515/CORRREV-2018-0102

[17] Marquez, A., Singh, J., Maharaj, C. (2021). Corrosion under insulation examination to prevent failures in equipment at a petrochemical plant. Journal of Failure Analysis and Prevention, 21(3): 723-732. https://doi.org/10.1007/S11668-021-01135-5

[18] Watt, C., Paterson, S., White, C., Wilk, T.P. (2021). Using industry data to develop improved methods to manage corrosion under insulation. In the SPE International Oilfield Corrosion Conference and Exhibition, Virtual. https://doi.org/10.2118/205057-MS

[19] Zorina, A.A., Tyurin, A. (2022). Development of measures to reduce the thermal load of the environment in the production boiler house of the enterprise. In 2022 33th All-Russian Youth Exhibition of Innovations, pp. 139-146. https://doi.org/10.22213/ie022120

[20] Garay-Martinez, R., Jayan, B., Arregi, B. (2020). Design of a calorimetric test facility to replicate real boundary conditions in the Gulf countries. E3S Web of Conferences, 172: 11007. https://doi.org/10.1051/E3SCONF/202017211007

[21] Patil, S., Priya, V.R.K., Lakkaraju, R. (2024). Heat transport and flow structures in inclined circular enclosures. Physical Review Fluids, 9: 124305. https://doi.org/10.1103/physrevfluids.9.124305

[22] Bao, Y., Zhang, F., Cheng, J., Wang, Y., Guan, Y., Ren, J., Jin, F, Cheng, Y., Xie, W. (2023). Simulation on heat transfer and emergency protection of tanks in a tank farm under fire scenario. International Journal of Environmental Research and Public Health, 20(7): 5348. https://doi.org/10.3390/ijerph20075348

[23] Bahadori, A., Vuthaluru, H.B. (2010). A simple method for the estimation of thermal insulation thickness. Applied Energy, 87(2): 613-619.

https://doi.org/10.1016/J.APENERGY.2009.05.012
[24] Alsayaydeh, J.A.J., Khang, W.A.Y., Indra, W.A., Shkarupylo, V., Jayasundar, J. (2019). Development of smart dustbin by using apps. ARPN Journal of Engineering and Applied Sciences, 14(21): 3703-3711.
[25] Huerta, F., Vesovic, V. (2024). CFD modelling of the non-isobaric evaporation of cryogenic liquids in storage tanks. Applied Energy, 356: 122420. https://doi.org/10.1016/j.apenergy.2023.122420
[26] Hwang, J. (2023). Daytime radiative cooling under extreme weather conditions. Advanced Energy and Sustainability Research, 5(5): 2300239. https://doi.org/10.1002/aesr.202300239
[27] Huo, W., Zhao, M., Wang, G. (2022). Analysis of gap heat loss in external thermal insulation system of passive low-energy-consumption building based on CFD. Journal of Building Performance Simulation, 16(1): 1-15. https://doi.org/10.1080/19401493.2022.2104374
[28] Alsayaydeh, J.A., Nj, M., Syed, S.N., Yoon, A.W., Indra, W.A., Shkarupylo, V., Pellipus, C. (2019). Home appliances control using Bluetooth. ARPN Journal of Engineering and Applied Sciences, 14(19): 3344-3357.
[29] Awanto, C., Houngan, A.C., Anjorin, M. (2014). Investigation of the optimal heat flux density for the refrigerated warehouses design. In 2014 International Conference and Utility Exhibition on Green Energy for Sustainable Development (ICUE), Pattaya, Thailand, pp. 1-6.
[30] Aasen, A., Blakseth, S.S., Massing, A., Nekså, P., Gjennestad, M.A. (2025). Thermal performance estimation for cryogenic storage tanks: Application to liquid hydrogen. International Journal of Hydrogen Energy, 144: 42-54. https://doi.org/10.48550/arxiv.2501.18451
[31] Jerman, M., Černý, R. (2012). Effect of moisture content on heat and moisture transport and storage properties of thermal insulation materials. Energy and Buildings, 53: 39-46. https://doi.org/10.1016/J.ENBUILD.2012.07.002
[32] Alsayaydeh, J.A.J., Indra, W.A., Khang, A.W.Y., Shkarupylo, V., Jkatisan, D.A.P.P. (2019). Development of vehicle ignition using fingerprint. ARPN Journal of Engineering and Applied Sciences, 14(23): 4045-4053.
[33] Colinart, T. (2023). Thermal conductivity assessment of moist building insulation material using a heat flow meter apparatus. Building and Environment, 234: 110184. https://doi.org/10.1016/j.buildenv.2023.110184
[34] Berardi, U., Zaidi, S. (2019). Characterization of commercial aerogel-enhanced blankets obtained with supercritical drying and of a new ambient pressure drying blanket. Energy and Buildings, 198: 542-552. https://doi.org/10.1016/J.ENBUILD.2019.06.027
[35] Mazrouei-Sebdani, Z., Naeimirad, M., Peterek, S., Begum, H., Galmarini, S., Pursche, F., Baskin, E., Zhao, S.Y., Gries, T., Malfait, W.J. (2022). Multiple assembly strategies for silica aerogel-fiber combinations–A review. Materials & Design, 223: 111228. https://doi.org/10.1016/j.matdes.2022.111228
[36] Alsayaydeh, J.A.J., Irianto, Zainon, M., Baskaran, H., Herawan, S.G. (2022). Intelligent interfaces for assisting blind people using object recognition methods. International Journal of Advanced Computer Science and Applications, 13(5): 84-92. doi:10.14569/IJACSA.2022.0130584
[37] Lakatos, Á. (2017). Investigation of the moisture induced degradation of the thermal properties of aerogel blankets: Measurements, calculations, simulations. Energy and Buildings, 139: 506-516. https://doi.org/10.1016/J.ENBUILD.2017.01.054
[38] Vevere, L., Yakushin, V., Sture-Skela, B., Andersons, J., Cabulis, U. (2024). Cryogenic insulation, towards environmentally friendly polyurethane foams. Polymers, 16(17): 2406. https://doi.org/10.3390/polym16172406
[39] Al-Andoli, M.N., Irianto, Alsayaydeh, J.A., Alwayle, I.M., Che Ku Mohd, C.K.N., Abuhoureyah, F. (2024). Robust overlapping community detection in complex networks with graph convolutional networks and fuzzy C-means. IEEE Access, 12: 70129-70145. https://doi.org/10.1109/ACCESS.2024.3399883
[40] Feng, M., Zhang, M., Pei, W., Chen, L. (2023). Correction of the thermal conductivity of polyurethane insulation material under freeze-thaw and water absorption conditions and its application. Cold Regions Science and Technology, 211: 103859. https://doi.org/10.1016/j.coldregions.2023.103859
[41] Alsayaydeh, J.A.J., Irianto, Aziz, A., Xin, C.K., Hossain, A.K.M.Z., Herawan, S.G. (2022). Face recognition system design and implementation using neural networks. International Journal of Advanced Computer Science and Applications, 13(6): 519-526. https://doi.org/10.14569/IJACSA.2022.0130663
[42] Fan, Y.G., Zhang, B., Zhang, Y. (2023). Optimal design of cryogenic insulation system for large liquefied natural gas (LNG) storage tanks based on operation factors. E3S Web of Conferences, 385: 03010. https://doi.org/10.1051/e3sconf/202338503010
[43] Wang, Y., Ma, C., Liu, Y., Wang, D., Liu, J. (2018). Effect of moisture migration and phase change on effective thermal conductivity of porous building materials. International Journal of Heat and Mass Transfer, 125: 330-342. https://doi.org/10.1016/J.IJHEATMASSTRANSFER.2018.04.062
[44] Seto, R. (2024). Mineral wool CUI mitigation improvements. Materials Performance, 63(8): 46-51. https://doi.org/10.5006/c2024-20798
[45] De Souza, M.P.V., López, F., Maldague, X. (2024). Corrosion under insulation mitigation by passive multivariate thermography. Quantitative InfraRed Thermography, 22(2): 121-133. https://doi.org/10.1080/17686733.2024.2305917
[46] Shi, X., Gong, G., Wang, Y., Huang, Y., An, J., Wang, H. (2024). Experimental and a dual-scale analysis of the influence of coating on humidity control ability of hygroscopic materials with different porosity. Construction and Building Materials. https://doi.org/10.1016/j.conbuildmat.2024.136163
[47] Scherbin, S., Glotov, V. (2025). Selection of material and thickness of thermal insulation. Scientific Papers Collection of the Angarsk State Technical University, 2025(1): 110-113. https://doi.org/10.36629/2686-7788-2025-1-110-113
[48] Arulrajah, A., Disfani, M.M., Maghoolpilehrood, F., Horpibulsuk, S., Udonchai, A., Imteaz, M., Du, Y.J. (2015). Engineering and environmental properties of foamed recycled glass as a lightweight engineering material. Journal of Cleaner Production, 94: 369-375. https://doi.org/10.1016/J.JCLEPRO.2015.01.080
[49] Fedorov, A.G., Pilon, L. (2002). Glass foams: Formation,

transport properties, and heat, mass, and radiation transfer. Journal of Non-Crystalline Solids, 311(2): 154-173. https://doi.org/10.1016/S0022-3093(02)01376-5

[50] Hassan, A.M., Bunnori, N.M., Ramesh, S., Tan, C.Y., Mo, K.H. (2024). Glass-based foam from alkali activation: A review on effect of primary foaming parameters on microstructure and density. Construction and Building Materials, 427: 136157. https://doi.org/10.1016/j.conbuildmat.2024.136157

[51] Shkarupylo, V., Blinov, I., Chemeris, A., Dusheba, V., Alsayaydeh, J.A.J., Oliinyk, A. (2021). Iterative approach to TLC model checker application. In Proceedings of the 2021 IEEE 2nd KhPI Week on Advanced Technology (KhPIWeek), Kharkiv, Ukraine, pp. 283-287. https://doi.org/10.1109/KhPIWeek53812.2021.9570055

[52] Berardi, U. (2019). The impact of aging and environmental conditions on the effective thermal conductivity of several foam materials. Energy, 182: 777-794. https://doi.org/10.1016/J.ENERGY.2019.06.022

[53] Alsayaydeh, J.A.J., Irianto, Ali, M.F., Al-Andoli, M.N.M., Herawan, S.G. (2024). Improving the robustness of IoT-powered smart city applications through service-reliant application authentication technique. IEEE Access, 12: 19405-19417. https://doi.org/10.1109/ACCESS.2024.3361407

[54] Churchill, S.W., Bernstein, M. (1977). A correlating equation for forced convection from gases and liquids to a circular cylinder in crossflow. Journal of Heat Transfer, 300-306. https://doi.org/10.1115/1.3450685

[55] Jeong, S.J., Lee, S.J., Moon, S.J. (2023). CFD thermo-hydraulic evaluation of a liquid hydrogen storage tank with different insulation thickness in a small-scale hydrogen liquefier. Fluids, 8(9): 239. https://doi.org/10.3390/fluids8090239

[56] Mavromatidis, L.E., Michel, P., El Mankibi, M., Santamouris, M. (2010). Study on transient heat transfer through multilayer thermal insulation: Numerical analysis and experimental investigation. Building Simulation, 3(4): 279-294. https://doi.org/10.1007/S12273-010-0018-Z

[57] Omle, I., Askar, A.H., Kovacs, E., Bolló, B. (2023). Comparison of the performance of new and traditional numerical methods for long-term simulations of heat transfer in walls with thermal bridges. Energies, 16(12): 4604. https://doi.org/10.3390/en16124604

[58] Dolgun, G.K., Keçebaş, A., Ertürk, M., Daşdemir, A. (2023). Life cycle cost assessment for thermal insulation of above-ground spherical container with different capacities in hot fluid storage processes. Journal of Cleaner Production, 403: 136875. https://doi.org/10.1016/j.jclepro.2023.136875

[59] Hasan, A. (1999). Optimizing insulation thickness for buildings using life cycle cost. Applied Energy, 63(2): 115-124. https://doi.org/10.1016/S0306-2619(99)00023-9

[60] Kotov, E.V., Nemova, D., Sergeev, V., Dontsova, A., Koriakovtseva, T., Andreeva, D. (2024). Thermal performance assessment of aerogel application in additive construction of energy-efficient buildings. Sustainability, 16(6): 2398. https://doi.org/10.3390/su16062398

[61] Ozel, M. (2012). Cost analysis for optimum thicknesses and environmental impacts of different insulation materials. Energy and Buildings, 49: 552-559. https://doi.org/10.1016/j.enbuild.2012.03.002